

A brain-penetrant microtubule-targeting agent that disrupts hallmarks of glioma tumorigenesis

Eric A. Horne, Philippe Diaz, Patrick J. Cimino, Erik Jung, Cong Xu, Ernest Hamel, Michael Wagenbach, Debra Kumasaka, Nicholas B. Wageling, Daniel D. Azorín, Frank Winkler, Linda G. Wordeman, Eric C. Holland and Nephi Stella

Pages 1-2: Tables of Contents

Supplementary Figures

Page 3 - Figure S1: Synthesis and analytics of (9-ethyl-9*H*-carbazol-3-yl)(quinolin-5-yl)methanol (ST-401).

Page 4 - Figure S2: MGG8 and T98G cells in culture have similar proliferation rates.

Page 5 - Figure S3: Twenty-four hours treatment with Y-27632, ST-401 and NOC does not affect viability of PD-glioma in culture.

Page 6 - Figure S4: ST-401 stability in tested formulations.

Page 7 - Figure S5: Dose range finding indicated that ST-401 was well tolerated by mice for up to 20 d when treated twice daily with 20 mg/kg.

Page 8 - Figure S6: Quantitation of ST-401 in mouse plasma and brain tissue

Page 9 - Figure S7: ST-401, TMZ, RT treatments and their combination did not significantly change the number of cells undergoing apoptosis in a RCAS-Tva PDGFB glioma.

Page 10 - Figure S8: Representative images of RCAS-Tva PDGFB glioma that was immuno-stained for HA and the threshold that shows increase in tumor density triggered by ST-401 compared to CTR.

Page 11 - Figure S9: TMZ, RT and ST-401 increased tumor density in a RCAS-Tva PDGFB glioma.

Supplementary Methods

Page 12 - Methods S1: Maximal tolerated dose (MTD) and Dose-range finding (DRF); Xenograft mouse model; RCAS/tv-a PDGFB glioma mouse model.

Page 13 - Methods S2: Cells in culture; [³H]Colchicine binding to purified tubulin and tubulin assembly.

Page 14 - Methods S3: Live cell imaging of MT polymerization; Time-lapse microscopy.

Page 15 - Methods S4: Fluorescence immunocytochemistry.

Page 16 - Methods S5: Cell proliferation and viability; Tumor microtubes analysis.

Page 17 - Methods S6: Histological analysis; Quantification and Statistical Analysis.

Page 18 - References

Figure S1: Synthesis and analytics of (9-ethyl-9H-carbazol-3-yl)(quinolin-5-yl)methanol (ST-401).

A. ST-401 synthesis: solution of *tert*-butyllithium 1.5 M in pentane (9.3 mL, 14 mmol) was added dropwise in 20 min at -78°C to a solution of 3-bromo-9-ethyl-9H-carbazole (2.12 g, 7.7 mmol) dissolved in dry THF (50 mL). The solution was stirred at -78°C for 1 additional hour. A brownish precipitate formed. TLC in Cyclohexane/DCM 9/1: 100 % conversion (R_f starting material: 0.48, R_f ethylcarbazole: 0.56). A solution of quinoline-5-carbaldehyde (1.1 g; 7 mmol) dissolved in 50 mL of dry THF was added dropwise at -78°C in 15 min. The resulting solution was stirred at -78°C for 1.5 h. TLC Cyclohexane/EtOAc 5/5: 100 % conversion. 220 mL of saturated NH_4Cl solution was added. The product was then extracted with EtOAc (200 mL and then 50 mL). The organic phase were combined and washed with water (2X100 mL) and dried over MgSO_4 . Solution was concentrated under reduced pressure. Flash-chromatography on Isolera system of the crude mixture using a gradient EtOAc/cyclohexane afforded the pure product as a pale yellow solid. Yield: 1.54 g (62.4%). **B. ST-401 ^1H NMR** (500 MHz, CDCl_3) δ 8.85 (d, $J = 3.8$ Hz, 1H), 8.43 (d, $J = 8.6$ Hz, 1H), 8.14 (s, 1H), 8.10 (d, $J = 8.4$ Hz, 1H), 8.05 (d, $J = 7.8$ Hz, 1H), 7.85 (d, $J = 7.1$ Hz, 1H), 7.77 (t, $J = 7.8$ Hz, 1H), 7.47 (t, $J = 7.6$ Hz, 1H), 7.41 (t, $J = 8.5$ Hz, 2H), 7.35 (d, $J = 8.5$ Hz, 1H), 7.28 (t, $J = 4$ Hz, 1H), 7.21 (t, $J = 7.5$ Hz, 1H), 6.70 (d, $J = 3.6$ Hz, 1H), 4.35 (q, $J = 7.2$ Hz, 2H), 2.45 (d, $J = 3.8$ Hz, 1H), 1.42 (t, $J = 7.2$ Hz, 3H). **C. ST-401 ^{13}C NMR** (101 MHz, CDCl_3) δ 149.89, 148.75, 140.41, 140.04, 139.68, 133.74, 133.08, 129.53, 129.05, 126.07, 126.00, 125.08, 125.03, 123.11, 122.83, 120.85, 120.63, 119.28, 119.07, 108.75, 108.70, 74.12, 37.72, 13.94.

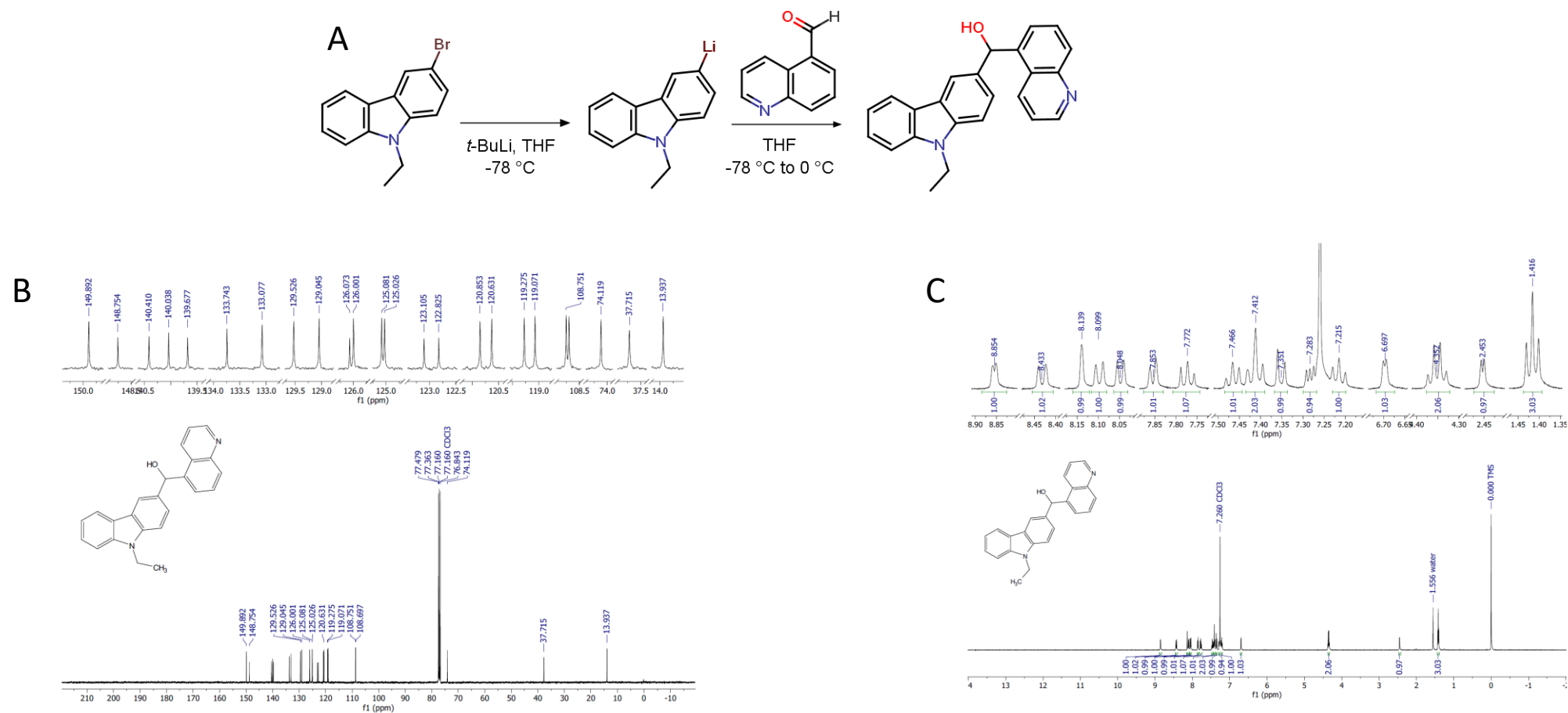


Figure S2: MGG8 and T98G cells in culture have similar proliferation rates.

Brd-U incorporation in MGG8 isolates and in T98G cells in culture was measured 2 h after seeding (Day 0) and after 72 h (Day 3). **A-B.** Three days in culture results in a 4.6-fold increase in the number of MGG8 cells in S phase (A) and a 4.0-fold increase in the number of T98G cells in S phase (B). Results are mean \pm S.E.M. from n = 7-15 experiments performed in triplicate.

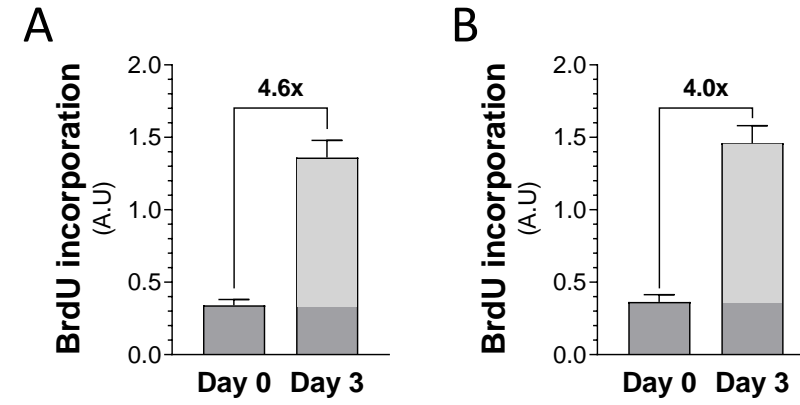


Figure S3: Twenty-four hours treatment with Y-27632, ST-401 and NOC does not affect viability of PD-glioma in culture.

Patient-derived glioma isolates (S24) in culture were treated with Y-27632, ST-401 and NOC for 24 h and change in cell viability was measured with Ho342 and EthD2 (see Figure 3). Y-27632 (50 μ M), ST-401 (300 nM) and NOC (300 nM) did not affect the cells death of S24 PD-glioma in culture. Results are mean \pm SEM (performed in triplicates and 3 ROIs per replicate). Two-way ANOVA analysis followed by Tuckey's post-test indicates no significant difference compared to basal (control) condition.

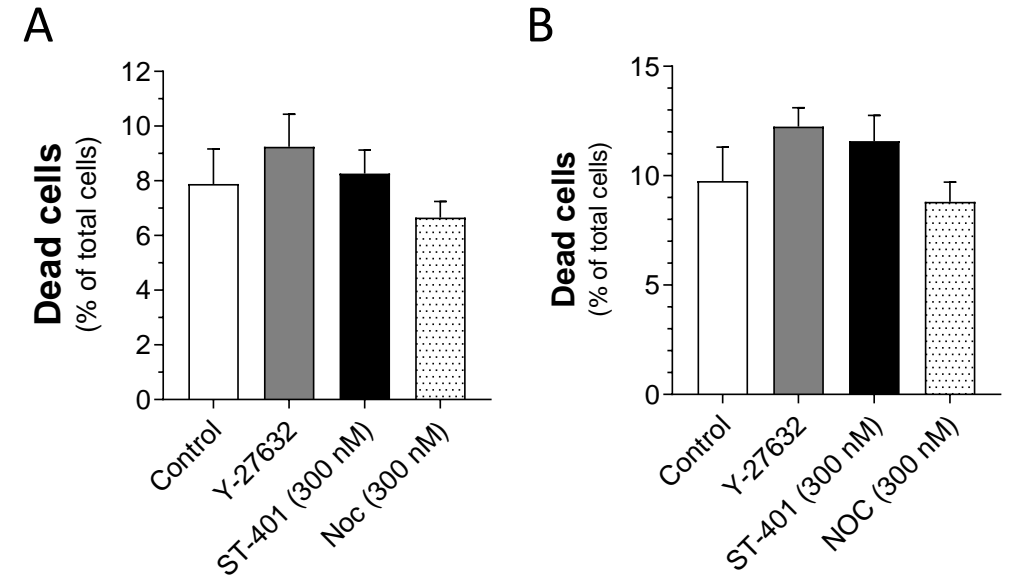


Figure S4: ST-401 stability in tested formulations.

Owing to its lipophilic nature, the stability of ST-401 dissolved at 20, 40, 60, 80 and 100 mM in select formulations was recorded initially and after 1, 3 and 7 days at -20 °C. The table shows results gathered with ST-401 (60 mM) at -20 °C for 7 d. Based on these results, we selected ethanol (EtOH):Cremophor RH40 (CRE):saline (DPBS) (1:2:17) as the formulation for our in vivo experiments. Thus, ST-401 was formulated as indicated in the table, and its solubility and stability at -20 °C initially and after 1, 4 and 7 days was determined (solubility verified visually by inspection using the following nomenclature of visual inspection : (S) remained in solution (i.e., clear solution), (N) not soluble (i.e., settling precipitates) and (P) partially soluble (i.e., cloudy solution). Each formulation was evaluated 3 times.

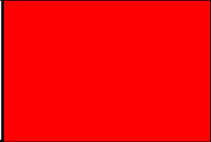



Pre-formulations	60 mM	
10% DMSO:DPBS		= insoluble
20% CRE:DPBS		= partially soluble
10% DMSO:20% CRE:DPBS		= soluble (clear liquid)
5%EtOH:10%CRE:DPBS (1:2:17)		

Figure S5: Dose range finding indicated that ST-401 was well tolerated by mice for up to 20 d when treated twice daily with 20 mg/kg.

ST-401 was injected i.p. in wild-type mice, and end stage, as indicated by signs of distress and toxicity, was recorded over time. Organs were harvested at end-stage of histology analysis.

A. Doses of ST-401 tested in the dose range finding (DRF) study inject once a day i.p. for 20 days (5 d/wk for 4 wk). **Green** indicates safe doses and **red** indicates non-safe doses (distress criteria are in Materials and Methods).

B. Normal weight gain of mice receiving vehicle control and ST-401 (5 mg/kg, 10 mg/kg and 20 mg/kg). Weight loss or no weight gain in mice receiving ST-401 50 mg/kg and 100 mg/kg, respectively. Mice receiving 150 mg/kg for two days were removed from the study because of end stage. Differences in initial weights are due to different animal cohorts.

C. Kaplan Meier survival curves of DRF study. Result from vehicle control and ST-401 (5 mg/kg, 10 mg/kg and 20 mg/kg) arms overlap at 100%. N = 4 mice per arm.

D. List of 6 organs that were harvested at end-stage, H&E stained and analyzed. No lesions signs and tissue toxicity was detected in these organs.

E. Doses of ST-401 tested in the dose range finding (DRF) study inject bidaily i.p. (bdip). **Green** indicates safe doses and **red** indicates non-safe doses (distress criteria are in Materials and Methods).

F. Normal weight gain of mice receiving vehicle control and weight loss or no weight gain in mice receiving ST-401 50 mg/kg and 100 mg/kg, respectively.

G. Kaplan Meier survival curves of DRF study. Result from vehicle control and ST-401 arms (50 mg/kg and 100 mg/kg).

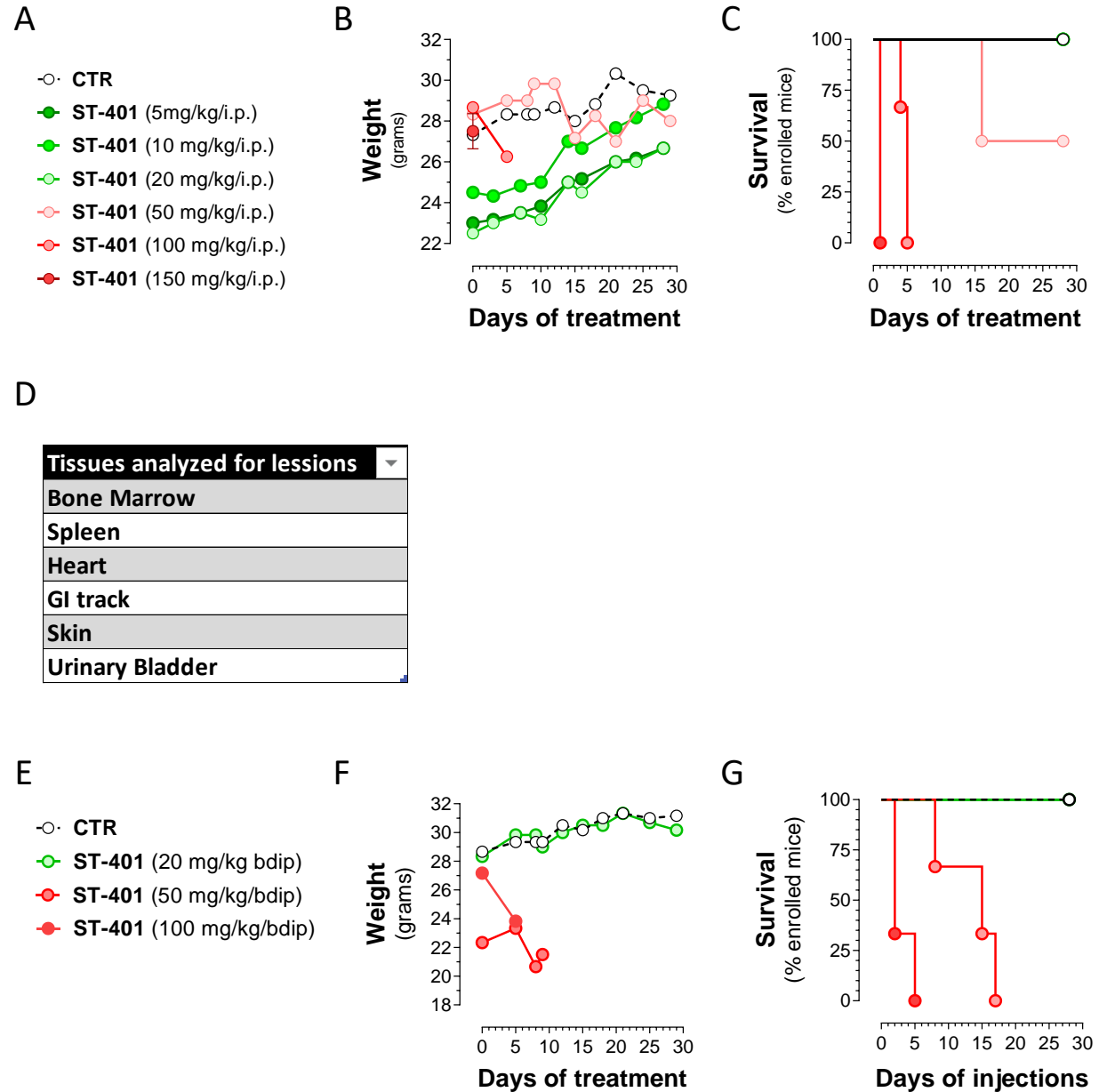


Figure S6: Quantitation of ST-401 in mouse plasma and brain tissue. Tissue samples were processed and analyzed at the University of Washington Mass Spectrometry Center. Between 135 and 461 mg of brain tissue was suspended in 1 mL PBS and homogenized to a fine slurry. Twenty μL of either undiluted plasma or brain homogenate were added to 10 μL of a 1 $\mu\text{g}/\text{mL}$ solution of the internal standard (2-methyl-1-propyl-1H-indol-3-yl)-1-naphthalenylmethanone (JWH-015).¹ The sample was vortexed, 70 μL of acetonitrile added, and the sample was vortexed again and centrifuged to sediment solids. Ten μL of supernatant were diluted with water to a final volume of 1 mL. One μL of the diluted sample was injected onto a Thermo Hypersil Gold C18 column (2.1x100 mm, particle size 1.7 μm) equilibrated with water/acetonitrile (55%/45%). ST-401 and internal standard were eluted with a linear gradient of acetonitrile in water (45% to 90%) at a flow rate of 0.3 mL/min. Mass spectrometric analysis was conducted on a Waters Xevo-TQS Triple quad using positive electrospray ionization. Retention times were 3.49 min for ST-401 and 4.02 min for JWH-015. Total run time was 6.5 min per sample. We monitored the transition of $m/z = 353.27$ to 158.063 for ST-401 and $m/z = 328.3$ to 155.1 for JWH-015. **A.** Areas under the curve for ST-401 were normalized to those of the internal standard and converted to tissue concentrations using a standard curve of ST-401 ranging from 12.5 to 3,800 ng/mL. Quality control standards were prepared by spiking plasma, brain and tissue homogenates with 250 and 1250 ng/mL of ST-401. Accuracy of the quality control standards was between 89 and 109%.

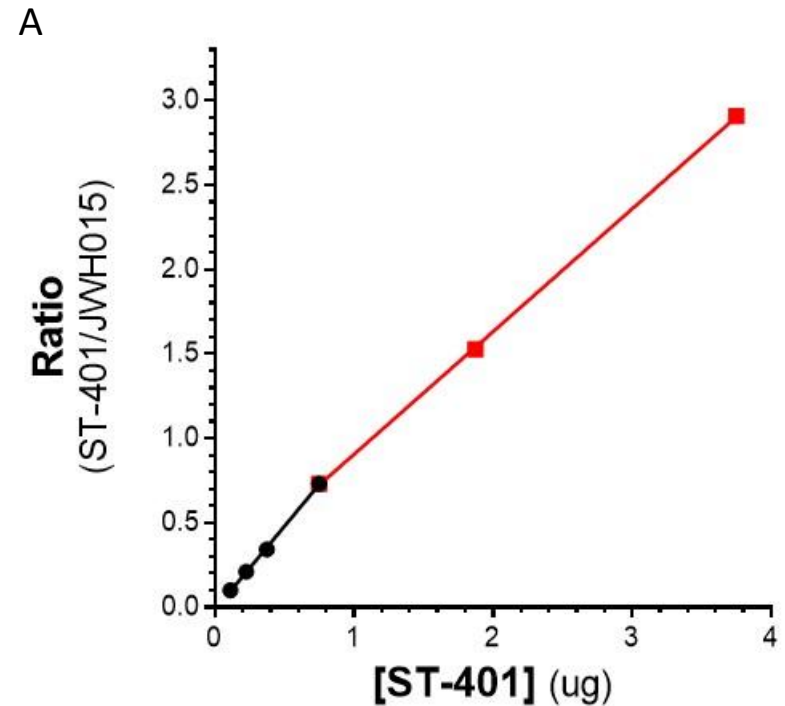


Figure S7: ST-401, TMZ, RT treatments and their combination did not significantly change the number of cells undergoing apoptosis in a RCAS-Tva PDGFB glioma.

Mouse brain harboring RCAS-Tva PDGFB glioma harvested at end stage (see Figure 5) were immunostained for cleaved caspase-3 (**caspase-3⁺**), and positively-stained particles were counted by unbiased semi-quantitative analysis using Image J.

A. ST-401, TMZ, RT treatments and their combination did not change the number of cells undergoing apoptosis in RCAS-Tva PDGFB glioma, as measured by quantifying caspase 3⁺ particles. Results are mean \pm S.E.M. from n = 16 images (8 brain sections in duplicate) from mice in the CTR and ST-401 arms, and n = 10 images (5 brain sections in duplicate) from mice in the RT, TMZ, ST-401+RT and ST-401+TMZ arms. Two-way ANOVA analysis followed by Tuckey's post-test indicated no significant difference.

B-C. Representative images of caspase-3⁺ immunoperoxidase staining showing large and small particles (yellow arrows) (B), and of the same area that was image processed (threshold and binary watershed) and particles counted by setting particle size (70-infinity; 0-1.0 circularity). Shown are 16x magnifications of original image of CTR arm. Scale bar = 20 μ m.

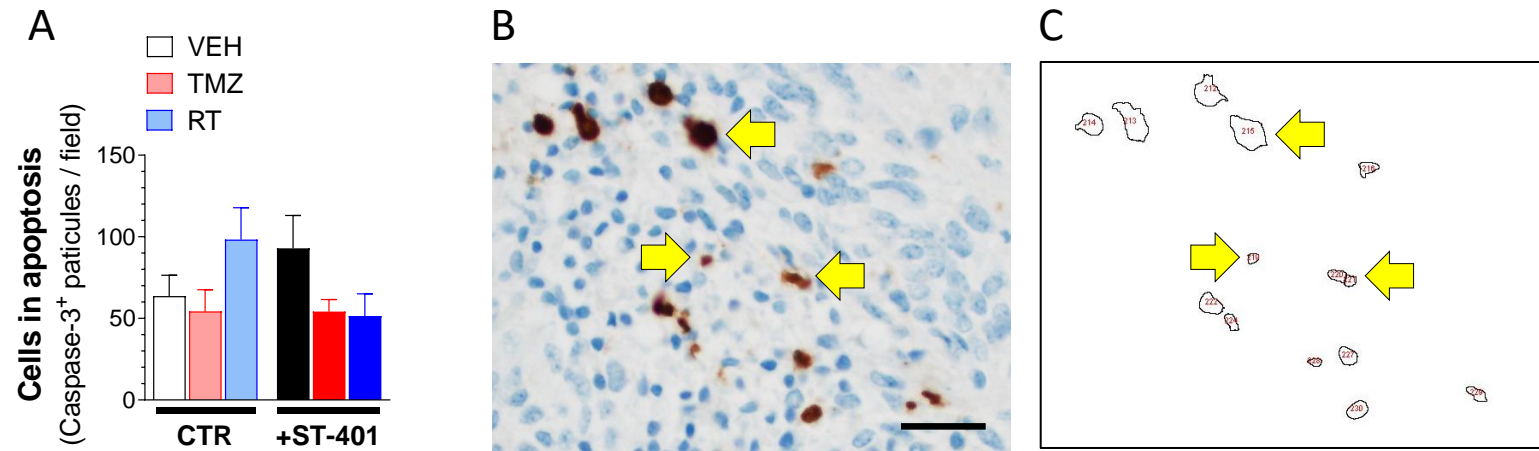
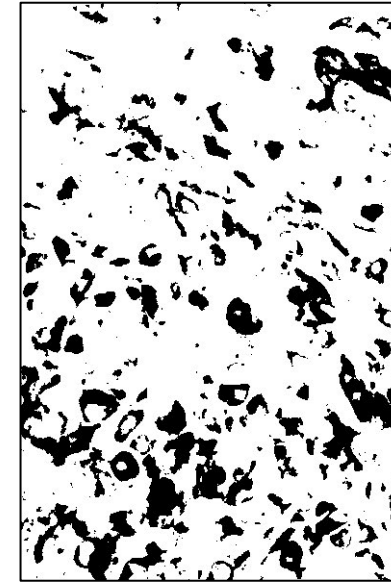


Figure S8: Representative images of RCAS-Tva PDGFB glioma that was immuno-stained for HA and the threshold that shows increase in tumor density triggered by ST-401 compared to CTR.

Mouse brain harboring RCAS-Tva PDGFB-driven glioma harvested at end stage (see figure 6) were immunostained for HA and % area of positively-stained pixels counted by unbiased semi-quantitative analysis using Image J. **A-B.** Example of threshold images of HA immunoperoxidase staining that were used to count the % area of positively-stained pixels of RCAS-Tva PDGFB-driven glioma sections in the CTR arm (A; threshold Figure 5F) and ST-401-treated arm (B; threshold Figure 5G).

A



B

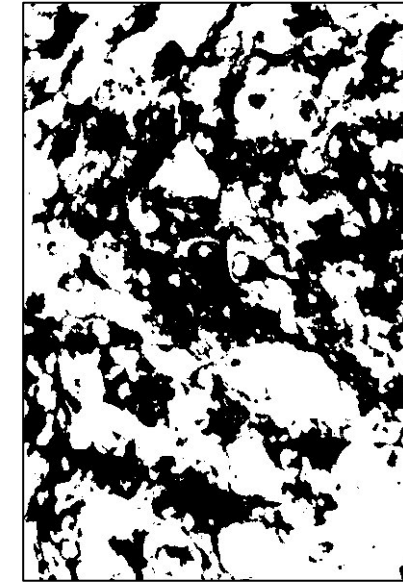
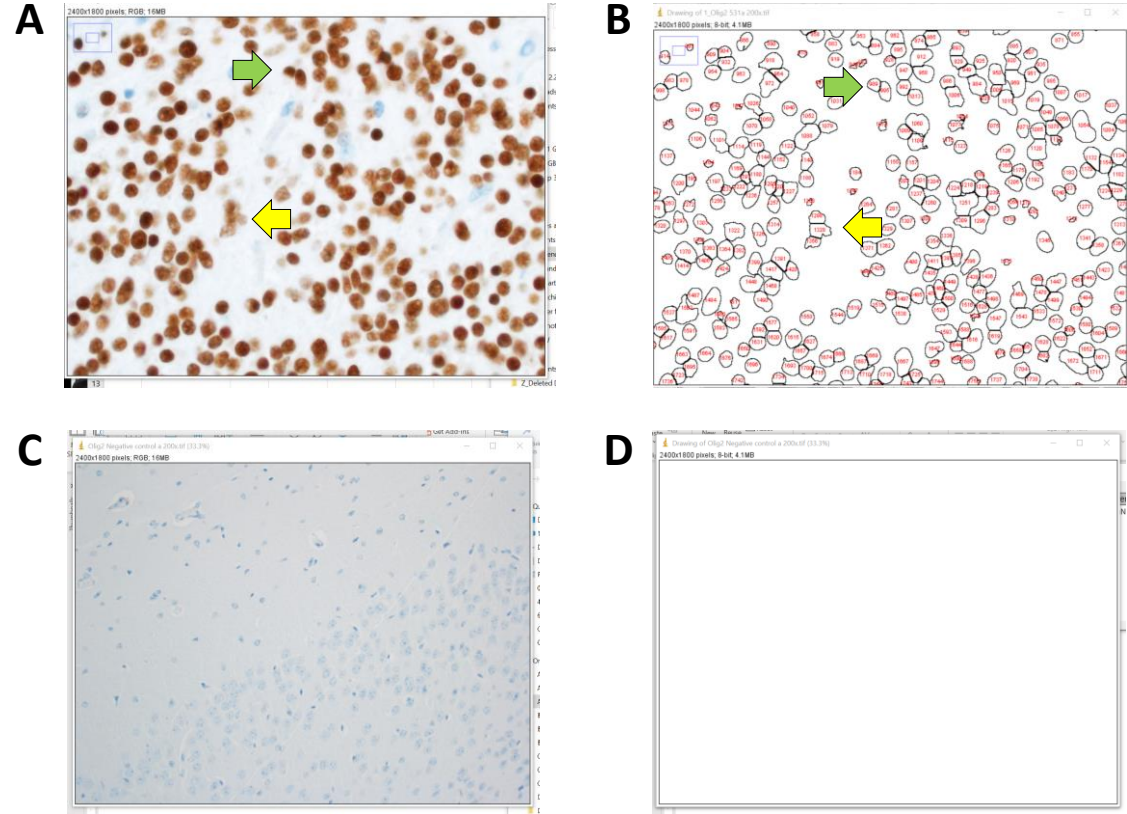


Figure S9: TMZ, RT and ST-401 increased tumor density in PDGFB-glioma.

Mouse brain harboring RCAS-Tva PDGFB-driven glioma harvested at end stage (see figure 6) were immunostained for **Olig-2**, and positively-stained particles were counted by unbiased semi-quantitative analysis using Image J.

A-D. Representative images of Olig-2 immunoperoxidase staining showing densely stained particles (green arrow) and moderately stained particles (yellow arrow) (A), and of the same area that was image processed (threshold, binary watershed and particles counted (particle size = 150 pixels-infinity; 0-1.0 circularity) (B). Representative images of peroxidase signal in negative staining brain sections (no primary antibody) (C) and of same image processed using the same setting and parameters, verify lack of quantification (D). Shown are 16x magnifications of original images.



Maximal tolerated dose (MTD) and Dose-range finding (DRF): study were performed following signs of general distress, including ataxia, squinting, piloerection, hunching, bradykinesia and dyspnea, monitoring for organ dysfunction and/or moribund state. Mice were then euthanized, and organs were harvested for H&E histopathological analysis by a board-certified veterinary pathologist (Dr. Denny Liggitt, Dept. of Comparative Medicine, University of Washington) who was blinded to group assignment.

Xenograft mouse model. COLO205 cells (2×10^6) were implanted in the flank of *Nude* mice (10-14 weeks of age) (10 mice per treatment arm). Once tumors reached 150 mm^3 , mice were treated with either formulation only (CTR) or ST-401 (regimen 2), and tumor growth measured using a caliper. End stage was reached when tumor volume $> 3000 \text{ mm}^3$.

RCAS/tv-a PDGFB glioma mouse model. The RCAS/tv-a system used in this study has been described¹⁻³. Briefly, four to six-week old *N/tv-a;Cdkn2a(Ink4a-Arf)^{-/-};Pten^{fl/fl}* mice underwent a stereotactic intracranial injection of 2×10^4 DF-1 cells with the RCAS virus (PDGFB-HA), in the SVZ region to generate GBM tumors. The mice were observed until they developed brain tumor related-symptoms, such as weight loss or general malaise. The mice were then entered into the appropriate treatment arms as described: 10 mice per arm. Mice were monitored throughout the study, euthanized at a humane endpoint and brains harvested for IHC analysis (see below).

Cells in culture. COLO205 and HCT116 cells (ATCC, Manassas, VA) were authenticated by ATCC when purchased using human short tandem repeat analysis and maintained in culture for less than 6 months. Cells were cultured in DMEM supplemented with 1% FBS, 100 U/mL penicillin, and 100 µg/mL streptomycin at 37 °C in a 5% CO₂ humidified atmosphere. HCT116 cells expressing EB1-EGFP from the genomic locus were generated by CRISPR/Cas9-directed recombination. Recombination template DNA was prepared containing the last intron and exon of EB1, followed by a 7-codon linker, the EGFP gene, and 3' untranslated chromosomal sequence. Chromosomal sequences near the EB1 stop codon were analyzed with the program CRISPRdirect (<http://crispr.dbcls.jp/>) to identify target sites. The targeting sequence 5'-CGATGTTGCTCTGCTGGTCC-3' was cloned into Cas9 plasmid pX459 version 2 (AddGene, Boston MA). Cells were co-transfected with linearized template DNA and Cas9 targeting vector. Proneuronal, mesenchymal and classical PD-glioma cells were a generous gift from Swedish Medical Center (Seattle, WA).⁴ MGG8 was a generous gift from Samuel Rabkin, Massachusetts General Hospital (Harvard, MA).⁵ PD-glioma cells were maintained in NeuroCult® NSA medium (Stem Cell Technologies) with B-27 serum-free supplement, 20 ng/mL epidermal growth factor and 20 ng/mL fibroblast growth factor 2 as described.^{6,7}

[³H]Colchicine binding to purified tubulin and tubulin assembly. [³H]Colchicine binding to purified tubulin and tubulin assembly (as assessed by turbidity development in purified bovine brain tubulin solutions) were both measured as described previously.⁸

Live cell imaging of MT polymerization. Beginning 24 h post-transfection, HCT116 transfected cells were selected for 48 h by treatment with 0.45 $\mu\text{g}/\text{mL}$ puromycin. Surviving cells were cloned by seeding at limiting dilution in a 50 mm glass-bottomed dish (MatTek) and EGFP-expressing colonies were selected on an inverted fluorescence microscope (Nikon). Genomic DNA from clones of recombinant cells was analyzed by PCR to confirm correct integration of EGFP into the EB1 locus. Lysates of cells were analyzed by Western blot with anti-EGFP and anti-EB1 antibodies to confirm expression of the fusion protein. HCT116 cells expressing EB1-GFP to label assembling MTs were imaged at a single Z-plane at 500-ms intervals at on a Deltavision microscope system (Applied Precision, Issaquah, WA) using a 60 \times 1.42 NA lens (Olympus, Tokyo, Japan).

Time-lapse microscopy. HCT116 cells stably expressing H2B-mCherry were plated in 35 mm HiQ4 4 chamber glass bottom imaging dishes at a density of 10,000 cells per chamber to visualize nuclei during live cell imaging. Immediately before imaging, media was replaced with CO₂-independent media containing agents. Images were acquired on a Nikon Biostation IM-Q (Nikon) as stacks of 4 \times 3- μm Z-steps every 5–10 min for 24–30 h. Alternatively, cells were cultured in glass-bottom 24 multi-well plates from Ibidi. After changing media to CO₂-independent media with reagents, cells were imaged using a GE InCell 2500 system with a 20x lens. Time-lapse images were collected as 15 μm Z-stack series, with 3 μm Z-spacing, and with 10 min time intervals for 24 h. Time-lapse movies were analyzed by hand using Fiji.

Fluorescence immunocytochemistry. Mitotic cells in Figure 2B: HCT cells were treated with ST-401 for 4 h at 37°C. After treatment, cells were fixed in 2% paraformaldehyde in Methanol at -20°C for 10 min. Tubulin and centrosomes were labeled using the anti-tubulin monoclonal DM1-alpha (1:250, Sigma) and anti-pericentrin (1:250, abcam) applied overnight at room temperature. Alexa-fluor 488 and 647 secondary antibodies against mouse and rabbit were used to detect the anti-tubulin and anti-pericentrin antibodies. Coverslips were mounted using ProLong® Gold containing DAPI (Molecular Probes, Eugene, OR). Fluorescent images were collected as 0.5- μ m Z-stacks on a Deltavision microscope system (Applied Precision/GEHealthcare, Issaquah, WA) using a 60 \times 1.42 NA lens (Olympus, Tokyo, Japan). Selected images were deconvolved using SoftWorx 5.0 (Applied Precision/GEHealthcare), and representative images are presented as a flat Z-projection. Interphase cells in Figure 2C: HCT cells were treated with ST-401 for 24 h at 37°C. After treatment, cells were fixed in 4% paraformaldehyde in PBS at 37°C for 15 min, and permeabilized in 0.5% Triton X-100 in PBS for 5 min at room temperature. Tubulin was labeled using the anti-tubulin monoclonal DM1-alpha (1:250, Sigma) applied overnight at room temperature. Alexa-fluor 488 secondary antibody against mouse was used to detect the anti-tubulin antibody. Coverslips were mounted using ProLong® Gold containing DAPI (Molecular Probes, Eugene, OR). Fluorescent images were collected using InCell 2500 system (GE Healthcare) with a 40X lens.

Cell proliferation and viability. WST-1 (Roche) and Brd-U (Sigma) staining was used to evaluate cell viability as described.⁹ Seventy two h following drug treatment according to the manufacturer's protocol. Maximal killing activity was identified as the maximal % reduction in cell viability measured at the drug concentrations tested. EC₅₀ values were calculated and reported only when a curve was reliably extrapolated by Prism software. The solvent for all modified carbazoles was DMSO (0.1% final). This solvent (negative reference, vehicle control) had no effect on cell viability. was measured as described by the manufacturer's instructions. WST-1 (Roche, Pleasanton, CA) was used to evaluate cell viability.

Tumor microtubes analysis. GFP-expressing, patient-derived S24 and BG5 cells were cultured under serum-free stem-like conditions as described previously.^{10,11} Cells were singularized using Accutase (A6964, Sigma-Aldrich) and seeded in Matrigel-coated (Matrigel® Growth Factor Reduced, 356231, Corning) 96-well plates. Twenty four h after seeding, compounds (DMSO control (0.125%), Y-27632 (72304, STEMCELL Technologies), nocodazole (12-281-0, Tocris Bioscience) and ST-401, all diluted in DMSO) were added to the media (DMEM-F12 medium (31330-038, Invitrogen), B27 supplement (12587-010, Invitrogen), 5 µg ml⁻¹ insulin (I9278, Sigma-Aldrich), 5 µg ml⁻¹ heparin (H4784, Sigma-Aldrich). Cells were treated for another 24 h before being stained with Hoechst-33342 (H3570, ThermoFisher) and Ethidium Homodimer-2 (EthD2) (E3599, ThermoFisher). Images were acquired using a Leica TCS SP5 confocal microscope. Analyses were performed semi-automatically using the pixel classification and object quantification workflows in ilastik software after appropriate training with control datasets.¹²

Histological analysis. Maximal mitotic figures for each slide were reviewed and two areas of highest mitotic activity were quantified for mitoses per region of interest (0.24 mm²).¹³ Similarly, areas of maximal tumor necrosis were quantified using the same parameters as for mitoses. Automated immunohistochemical staining processing (Discovery, Ventana Medical Systems, Inc.) was performed using the manufacturer's standard protocol. The following primary antibodies were used: HA tag (1:2000, Rb, Cell Signaling, c29F4), Olig2 (1:400, Rb, EMD millipore, Ab9610), and cleaved caspase 3 (1:300, Rb, Cell Signaling, 9662). For semi-quantitative IHC analysis, tissue sections were analyzed using ImageJ. Specifically, 200x images of tissue sections were converted to 8 bytes type images and their threshold adjusted using set parameters for each antibody (see examples provided in Figures S9-S11). Images were then converted to binary data and particles outlined using Watershed function, and particle size was set for each antibody counted automatically by excluding edges.

Quantification and Statistical Analysis. All of the statistical details of experiments can be found in figure legends. For all comparisons between two groups of independent datasets, multiple t tests were performed, p value, mean and standard error of the mean (SEM) were reported. For all comparisons among more than two groups (>2), one-way or two-way ANOVA were performed, p values and SEM were reported; and p values were adjusted by multiple testing corrections (Tuckey's post-test) when applicable. For all figures, *** represents p<0.001. ** represents p<0.01 and * represents p<0.05. The usage of all statistical approaches was examined using Graph Pad Prism (version 8).

References:

1. Holland EC, Celestino J, Dai C, Schaefer L, Sawaya RE, Fuller GN. Combined activation of Ras and Akt in neural progenitors induces glioblastoma formation in mice. *Nature genetics*. 2000; 25(1):55-57.
2. Holland EC, Hively WP, DePinho RA, Varmus HE. A constitutively active epidermal growth factor receptor cooperates with disruption of G1 cell-cycle arrest pathways to induce glioma-like lesions in mice. *Genes & development*. 1998; 12(23):3675-3685.
3. Holland EC, Varmus HE. Basic fibroblast growth factor induces cell migration and proliferation after glia-specific gene transfer in mice. *Proceedings of the National Academy of Sciences*. 1998; 95(3):1218-1223.
4. Diaz P, Horne E, Xu C, et al. Modified carbazoles destabilize microtubules and kill glioblastoma multiform cells. *European Journal of Medicinal Chemistry*. 2018.
5. Wakimoto H, Kesari S, Farrell CJ, et al. Human glioblastoma-derived cancer stem cells: establishment of invasive glioma models and treatment with oncolytic herpes simplex virus vectors. *Cancer research*. 2009; 69(8):3472-3481.
6. Pollard SM, Yoshikawa K, Clarke ID, et al. Glioma stem cell lines expanded in adherent culture have tumor-specific phenotypes and are suitable for chemical and genetic screens. *Cell stem cell*. 2009; 4(6):568-580.
7. Hothi P, Martins TJ, Chen L, et al. High-throughput chemical screens identify disulfiram as an inhibitor of human glioblastoma stem cells. *Oncotarget*. 2012; 3(10):1124.
8. Fung S, Xu C, Hamel E, et al. Novel indole-based compounds that differentiate alkylindole-sensitive receptors from cannabinoid receptors and microtubules: Characterization of their activity on glioma cell migration. *Pharmacol Res*. 2016.
9. Cherry AE, Haas BR, Naydenov AV, et al. ST-11: a new brain-penetrant microtubule-destabilizing agent with therapeutic potential for glioblastoma multiforme. *Mol Cancer Ther*. 2016; 15(19):2018-2029.
10. Osswald M, Jung E, Sahm F, et al. Brain tumour cells interconnect to a functional and resistant network. *Nature*. 2015; 528(7580):93.
11. Jung E, Osswald M, Blaes J, et al. Tweety-homolog 1 drives brain colonization of gliomas. *Journal of Neuroscience*. 2017; 37(29):6837-6850.
12. Berg S, Kutra D, Kroeger T, et al. ilastik: interactive machine learning for (bio) image analysis. *Nature Methods*. 2019:1-7.
13. Yoda RA, Marxen T, Longo L, et al. Mitotic Index Thresholds Do Not Predict Clinical Outcome for IDH-Mutant Astrocytoma. *Journal of Neuropathology & Experimental Neurology*. 2019; 78(11):1002-1010.